

# Polyoxometalate Ligands Reveal Different Coordination Chemistries Among Lanthanides and Heavy Actinides

Ian Colliard\* and Gauthier J.-P. Deblonde\*



Cite This: <https://doi.org/10.1021/jacsau.4c00245>



Read Online

ACCESS |

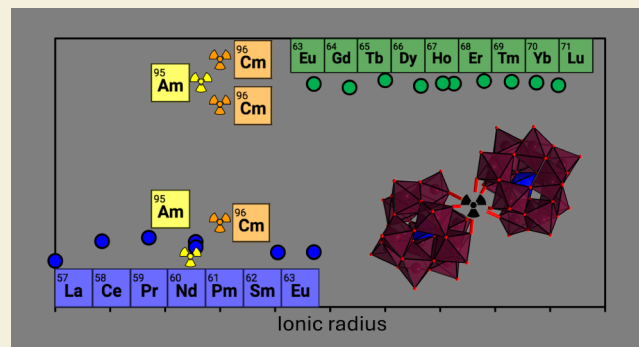
Metrics & More

Article Recommendations

Supporting Information

**ABSTRACT:** Experimental studies involving actinide compounds are inherently limited in scope due to the radioactive nature of these elements and the scarcity and cost of their research isotopes. Now, ~80 years after the introduction of the actinide concept by Glenn Seaborg, we still only have a limited understanding of the coordination chemistry of f-block metals when compared to more common elements such as the s-, p-, and d-blocks. This is particularly true for transplutonium actinides (Am, Cm, Bk, etc.) whose chemistry is often considered similar to trivalent lanthanides—mainly because of the lack of experimental data. We here report a metal–ligand system for which lanthanide and heavy actinide coordination compounds can be synthesized efficiently (i.e., requiring only a few micrograms) under identical conditions. Seventeen single crystal XRD structures of trivalent f-elements complexed to the polyoxometalate (POM)  $\text{PW}_{11}\text{O}_{39}^{7-}$  were obtained, including the full lanthanide series ( $\text{Cs}_{11}\text{Ln}(\text{PW}_{11}\text{O}_{39})_2 \cdot n\text{H}_2\text{O}$ , Ln = La to Lu, except Pm), the equivalent yttrium compound, a curium-POM compound ( $\alpha_2\text{-Cs}_{11}\text{Cm}(\text{PW}_{11}\text{O}_{39})_2 \cdot 33\text{H}_2\text{O}$ ), and the first two Am<sup>3+</sup>-POM compounds structurally characterized ( $\alpha_1\text{-Cs}_{11}\text{Am}(\text{PW}_{11}\text{O}_{39})_2 \cdot 6\text{H}_2\text{O}$  and  $\alpha_2\text{-Cs}_{11}\text{Am}(\text{PW}_{11}\text{O}_{39})_2 \cdot 21\text{H}_2\text{O}$ ). Importantly, this represents a unique series of compounds built on the same 1:2 metal:ligand unit and where all the f-elements are 8-coordinated and squared antiprismatic, thus providing a consistent platform for intra- and inter-series comparison. Despite a similar first coordination sphere environment, significant crystallographic and spectroscopic differences were observed among early and late lanthanides, as well as lanthanides and actinides, and even between americium and curium. These results show that even within the same coordination chemistry framework, 4f and 5f elements exhibit fundamental chemical differences that cannot be explained by simple size-match arguments. This study offers a versatile coordination platform to magnify differences within the f-block that have remained difficult to observe with traditional ligand systems.

**KEYWORDS:** actinides, polyoxometalates, lanthanides, f-elements, crystallography, raman, rare earths



## INTRODUCTION

Glenn T. Seaborg introduced the concept of the existence of an actinide element series about 80 years ago<sup>1</sup> and gave them their current place in the periodic table, below the lanthanides. However, despite the flourishing nuclear industry that has developed since then, chemical information on actinides is still very limited when compared to the rest of the periodic table. For instance, while >100,000 compounds have been structurally characterized for each of the common d-block metals (i.e., Fe, Zn, Cu, Co), or even >10,000 for each of the precious ones (i.e., Pt, Pd, Re, Ru, Ir, Os),<sup>2</sup> very few compounds containing actinides (An) other than uranium and thorium have been isolated and structurally characterized. To date, only ~50 single crystal XRD structures have been reported for Am compounds, ~10 for Cm, Bk, or Cf, and none for Ac or elements beyond californium.<sup>2,3</sup>

Since its inception, progress in actinide chemistry has been hindered by inherent experimental difficulties, such as radio-

activity constraints, high material cost, and scant isotope production. When considering the scale of compound syntheses, research isotope availability restricts it to just a few milligrams for americium, curium, berkelium, or californium, and a few micrograms or less for elements like actinium, einsteinium, and heavier elements.<sup>4</sup> In terms of radiological hazards, 1 mg of <sup>241</sup>Am is equivalent to approximately the same radioactivity level as 10 kg of pure <sup>238</sup>U and 1 mg of <sup>249</sup>Bk is as active as about 5000 kg of <sup>238</sup>U. Other nuclear effects such as criticality, spontaneous fissions, gamma, and neutron emissions also add to the radiological impact when handling transplutonium isotopes.

Received: March 15, 2024

Revised: April 26, 2024

Accepted: April 29, 2024

Actinides also exhibit acute chemical toxicity, with the lethal doses ( $LD_{50}$ ) in the submilligram range for transuranic elements.<sup>5,6</sup> All of the above severely limit the experimental scope of most studies, and novel approaches are needed to synthesize, isolate, and characterize in detail actinide compounds.

Traditional methods to study actinides involve using chemical analogues, with the 4f lanthanide (Ln) group being the most commonly used one. A more direct method involves the crystallization of actinide elements with small organic or inorganic chelators. The later method has yielded in the first two single crystal XRD structural data sets on  $Cf^{3+}$  in 2005 (iodate complex)<sup>7</sup> and 2015 (tris-chelate dipicolinate)<sup>8</sup> and then on  $Bk^{3+}$  in 2016 (also tris-chelate dipicolinate).<sup>9</sup> A handful of other  $Cf^{3+}$  and  $Bk^{3+}$  compounds were subsequently reported, at a pace of about one per year, and all were obtained from  $\sim 5$  mg scale syntheses (with borate,<sup>8</sup> iodate,<sup>10</sup> dioxophenoxazine,<sup>11</sup> dithiocarbamate,<sup>12</sup> mellitate,<sup>13,14</sup> terpyridyl,<sup>15</sup> metallocene,<sup>16</sup> and squarate-oxalate<sup>17</sup> ligands). A small number of  $Am^{3+}$  and  $Cm^{3+}$  compounds have similarly been crystallized with the same or similar small organic or inorganic chelators.<sup>18–23</sup> The first, and thus far the only,  $Bk^{4+}$  compound that has been structurally characterized is a tetraiodate complex reported in 2017.<sup>10</sup> The first structural characterization of a  $Cf^{2+}$  compound, with crown-ether ligand, was reported in 2023.<sup>24</sup> The only compounds containing an  $Am^{4+}$  or americyl ( $AmO_2^{2+}$ ) ion were characterized in 2009<sup>25</sup> and 2023,<sup>26</sup> respectively. However, such synthetic procedures required milligram amounts of the studied actinide isotope—for each structure—which severely limits the experimental space that can be investigated. This can generally explain the slow pace of development of heavy actinide chemistry and the dearth of experimental data published on actinide compounds relative to other elements. Any milligram-scale synthesis is also nontransposable to other, more radioactive, and elusive elements like actinium, promethium, einsteinium, etc. Despite the monumental progress in f-element chemistry that the aforementioned studies represent, their inherent logistical and experimental hurdles, combined with the diversity of ligands used, prevented the systematic investigation and comparison of lanthanide and actinide coordination chemistries within a consistent framework.

To address such issues, the use of high-molecular small molecules, specifically lacunary polyoxometalates (POMs), combined with optimized synthetic techniques, has recently lowered the amount of actinide material needed by 3 orders of magnitude, allowing synthesis, plus structural and spectroscopic characterization (single crystal XRD, Raman, UV-vis, etc.) from just a few micrograms instead of milligrams. Lacunary polyoxometalates (POMs) are ideally suited to study actinide elements, being versatile, high-molecular-weight ligands (>2000 g/mol). Moreover, POMs are radiation-resistant, and their structural and spectroscopic properties are driven by the metal center and can be tuned by the POMs' variety of sizes, shapes, and compositions. Despite their optimum characteristics, only one heavy actinide-POM compound was known until recently: the tetravalent americium complex with the  $P_2W_{17}O_{61}^{10-}$  POM, i.e.,  $[Am(P_2W_{17}O_{61})_2]^{16-}$ , isolated in 2009 starting from 2.5 mg of  $^{243}Am$ .<sup>25</sup>

In 2022, our team leveraged POMs to crystallize microgram quantities of curium (1–10  $\mu\text{g}$  of  $^{248}/^{246}\text{Cm}^{3+}$  per synthesis), producing the first three curium-POM complexes ever isolated.<sup>27</sup> Interestingly, our study, which also used selected lanthanide analogues to first confirm the POM-based synthesis

approach, quickly began to showcase divergent spectroscopic behaviors between lanthanide-POM and actinide-POM complexes. Most noticeably, the empirical Kimura equations<sup>28,29</sup> used to describe the relationship between lanthanide fluorescence lifetimes and hydration numbers could accurately describe the coordination of the Ln-POMs tested (e.g.,  $[Ln(W_5O_{18})_2]^{9-}$ ,  $[Ln(PW_{11}O_{39})_2]^{11-}$ ,  $[Ln(BW_{11}O_{39})_2]^{15-}$ , and  $[Ln(P_2W_{17}O_{61})_2]^{17-}$ , with an 8-coordinated  $Ln^{3+}$  and no binding water molecules). In contrast, the corresponding equations failed to describe the POM complexes<sup>27</sup> with  $Cm^{3+}$ , even though other spectroscopic techniques (e.g., Raman) mirrored the lanthanide counterparts. The solution-state NMR parameters of these actinide-POM complexes were also found to be distinct from their lanthanide analogues.<sup>30</sup> Prior structural studies on heavy actinides also often lacked a comprehensive comparison with the lanthanide series, focusing instead on just a few size-matched lanthanides or just the actinides. Changes in coordination chemistry along the lanthanide series for most metal–organic ligand complexes (e.g., change in the coordination number around the middle of the  $Ln^{3+}$  series or changes in the ligand's coordination mode) also complexify the interpretation of the data and comparison with the corresponding actinide compounds. As such, there is a need for a new direct examination of actinide elements, one that does not discount the shared chemistry of the lanthanides but improves upon the uniqueness of the actinide series, while acknowledging its radioactive nature and associated experimental limitations.

Herein, we provide a thorough structural analysis of the coordination chemistry of trivalent lanthanides and a direct comparison with americium and curium. The POM-based approach offers a consistent framework to synthesize both 4f- and 5f-element complexes under the same conditions. We show that single crystals of the  $[Ln(PW_{11}O_{39})_2]^{11-}$ ,  $[Am(PW_{11}O_{39})_2]^{11-}$ , and  $[Cm(PW_{11}O_{39})_2]^{11-}$  complexes can be reliably and efficiently obtained from micrograms of the starting material (Figure 1). In addition to a detailed solid-state Raman

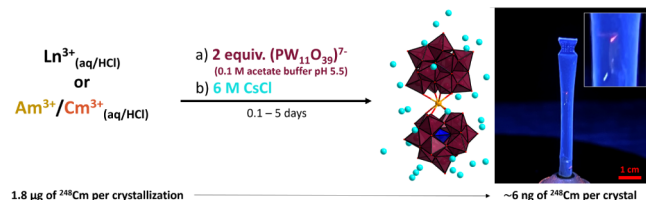


**Figure 1.** POM-based synthetic approach for crystallizing actinide complexes at the microgram scale. The picture on the right shows a single crystal of the new curium-POM ( $\alpha_2\text{-Cs}_{11}\text{Cm}(PW_{11}O_{39})_2 \cdot 33\text{H}_2\text{O}$ ) mounted on a crystallography pin and within a plastic sleeve for radiological containment. The  $Cm^{3+}$ -POM complex is fluorescent under UV light. The picture was taken in the dark under UV irradiation. The faint pink-orange glow of the single crystal was captured via a smartphone CCDC camera. Some dust particles on the plastic sleeve appear white under UV light.

spectroscopy analysis, we report 13 new crystal structures of  $Ln^{3+}$ -POM compounds ( $Cs_{11}Ln(PW_{11}O_{39})_2 \cdot n\text{H}_2\text{O}$ , with  $n = 3$  to 22), the equivalent yttrium compound ( $Cs_{11}\text{Y}(PW_{11}O_{39})_2 \cdot 13\text{H}_2\text{O}$ ), and a new curium-POM structure ( $\alpha_2\text{-Cs}_{11}\text{Cm}(PW_{11}O_{39})_2 \cdot 33\text{H}_2\text{O}$ ). We also report the first two  $Am^{3+}$ -POM compounds that were structurally characterized ( $\alpha_1\text{-Cs}_{11}\text{Am}(PW_{11}O_{39})_2 \cdot 6\text{H}_2\text{O}$  and  $\alpha_2\text{-Cs}_{11}\text{Am}(PW_{11}O_{39})_2 \cdot 21\text{H}_2\text{O}$ ). Importantly, all compounds contain an 8-coordinated square antiprism central cation and are built on the same unit 1:2

metal:POM complex. Despite similar first coordination sphere environment, significant crystallographic differences were observed between early and late lanthanides, as well as actinides and lanthanides, and even between americium and curium. These results show that even within the same coordination chemistry framework, 4f- and 5f-element series exhibit fundamental chemical differences that cannot be explained by simple size arguments.

## RESULTS AND DISCUSSION

### Structure of the Keggin Complexes with Actinides and Lanthanides

Briefly, the parent Keggin structure,  $[\alpha\text{-PW}_{12}\text{O}_{40}]^{3-}$  ( $\text{PW}_{12}$ ), of which  $[\alpha\text{-PW}_{11}\text{O}_{39}]^{7-}$  ( $\text{PW}_{11}$ ) is derived, comprises a central tetrahedral  $[\text{PO}_4]$  caged by 12 octahedral  $[\text{WO}_6]$  units, each linked to one another by the neighboring oxygen atoms (Figure 2). Due to the octahedral coordination of the  $[\text{WO}_6]$  units, two

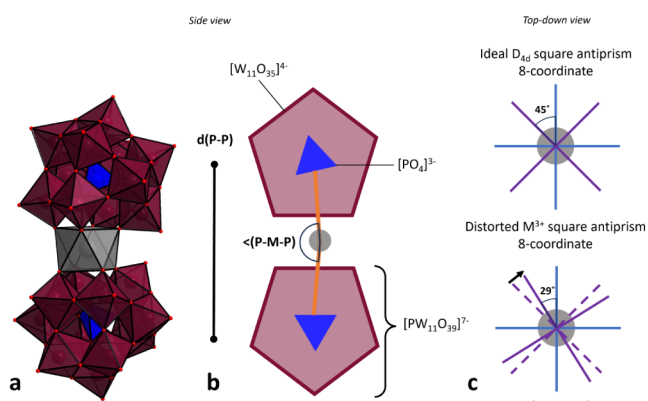


**Figure 2.** Structural parameters in f-element complexes with the POM  $\text{PW}_{11}\text{O}_{39}^{7-}$ . a) Polyhedral representation of  $\text{M}(\text{PW}_{11}\text{O}_{39})_2$ , Ln or An cation (M) in gray, W in maroon, and oxygen as red spheres. b) Side view projection of  $\text{M}(\text{PW}_{11}\text{O}_{39})_2$ , represented in simple geometric figures. Pentagons in maroon represent the  $[\text{W}_{11}\text{O}_{35}]^{4-}$  cage, blue triangles represent the encapsulated  $[\text{PO}_4]^{3-}$ , and the gray circles represent the central Ln or An cation. This projection thus showcases  $d(\text{P}-\text{P})$  as the distance between the triangles and  $\angle(\text{P}-\text{M}-\text{P})$  as the bending angle between the triangles and the sphere. c) Top-down projection highlighting only the central cation (e.g.,  $\text{Ln}^{3+}$  or  $\text{An}^{3+}$ ) as a circle with its corresponding eight bonds, and the distortion from an ideal 8-coordinate antiprism is defined as  $\angle(\text{P}-\text{MO}_8-\text{P})$ .

sets of O-bridging modes between  $[\text{WO}_6]$  units arise: corner-to-corner (only one O atom shared between  $[\text{WO}_6]$  units) and edge-to-edge (two O atoms shared between  $[\text{WO}_6]$  units). The 12 octahedral  $[\text{WO}_6]$  units can also be grouped into four sets of trimers. Each  $[\text{WO}_6]$  octahedron within a trimer is connected edge-to-edge, and connectivity between trimer sets is corner-to-corner. The isomeric nature of the Keggin structure arises from rotation of select trimers, changing the ratio of corner-to-corner and edge-to-edge. The four sets of trimers in the Keggin structure, each able to rotate by  $60^\circ$ , lead to a total of five potential isomers ( $\alpha$ ,  $\beta$ ,  $\gamma$ ,  $\delta$ , and  $\epsilon$ ). The  $\alpha$  isomer is the most thermodynamically stable one for tungstate POMs. Lacunary derivatives of the parent Keggin, primarily the  $\text{PW}_{11}$ , occur by removing one  $[\text{WO}]$  unit at pH values higher than 1.5. Herein, the precursor used,  $\text{Na}_4\text{PW}_9\text{O}_{34}\cdot n\text{H}_2\text{O}$ , converts in situ to the  $[\text{PW}_{11}\text{O}_{39}]^{7-}$  anion at pH 5.5.<sup>31,32</sup> Additionally, previous pH and NMR titration experiments<sup>30,33</sup> between  $\text{Ln}^{3+}$  and  $\text{PW}_{11}$  at a 1:2 ratio showcased that a pH of 5.5 leads to higher

complexation and stability of  $\text{Ln}(\text{PW}_{11})_2$ . Therefore, all experiments with lanthanide and actinide ions were conducted at a pH of 5.5 using microgram quantities (see Figure 1 and the Experimental Section for more information). As such, through identical synthesis procedures, consistent structural analysis of the  $\text{Cs-Ln}(\text{PW}_{11})_2$  and  $\text{Cs-An}(\text{PW}_{11})_2$  series can be conducted, as described below.

### Unexpected Structural Break within the Keggin-Lanthanide Complex Series

The lanthanide series provides the largest series of elements to systematically evaluate isomorphic parameters. Each  $\text{Cs-Ln}(\text{PW}_{11})_2$  crystal structure reported herein was grown through the same synthetic procedure in order to minimize the variables that could contribute to structural changes.  $\text{Y}^{3+}$  was added to this study as it exhibits a lanthanide-like chemistry and has a similar ionic radius to  $\text{Dy}^{3+}$  but has no f-electron.<sup>34</sup> As a result, we obtained a consistent series of structures with the same base formula of  $\text{Cs}_{11}\text{Ln}(\text{PW}_{11}\text{O}_{39})_2\cdot n\text{H}_2\text{O}$  ( $n = 2-21$ ) where  $\text{Ln} = \text{La}^{3+}$  through  $\text{Lu}^{3+}$  and  $\text{Y}^{3+}$ . Radioactive  $\text{Pm}^{3+}$  was not included here, as it will be reported in a separate case study. Tables S1–S3 give detailed crystallographic data collection information for each of these 17 structures reported herein (13 lanthanides, 1 with Y, plus 2 with Am, and 1 with Cm).

Despite a similar general formula, two distinct unit cells were identified, both crystallizing in space group  $P-1$  (Figure 3a). For

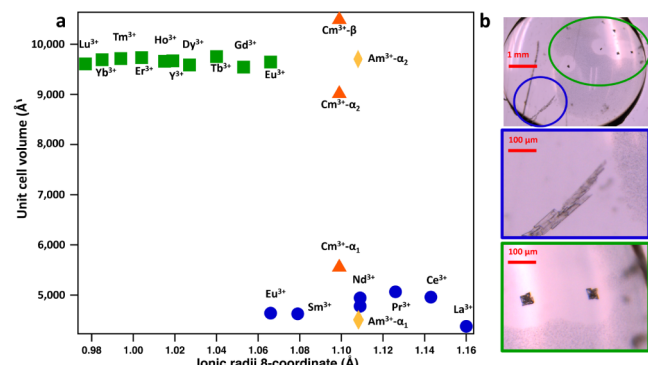


**Figure 3.** a) Unit cell volume change observed across the series of  $\text{Cs-Ln}(\text{PW}_{11})_2$  and  $\text{Cs-An}(\text{PW}_{11})_2$  ( $\text{An} = \text{Am}^{3+}$  or  $\text{Cm}^{3+}$ ). Structures with parallel stacking are shown with circle symbols ( $\text{Ln} = \text{La}^{3+}$  to  $\text{Eu}^{3+}$ ). Perpendicular stacking is shown in square symbols ( $\text{Ln} = \text{Eu}^{3+}$  to  $\text{Lu}^{3+}$ , plus  $\text{Y}^{3+}$ ). Americium ( $\text{Am}^{3+}$ , lozenges) crystallizes in perpendicular framework, although with some specificities—see text. Curium ( $\text{Cm}^{3+}$ , triangles) crystallizes in a parallel framework ( $\alpha_1$ ), with some specificities, and its own lattice arrangement ( $\alpha_2$ ) as well.  $\text{Cm}^{3+}$  also forms the  $\beta$  Keggin isomer, as previously reported.<sup>27</sup> For more information, see Tables S1–S3 and Figures S2–S4. b) Picture of the cocrystallization of the two  $\text{Cs-Eu}(\text{PW}_{11})_2$  structures (perpendicular and parallel frameworks) within the same sample.

the “light lanthanides” ( $\text{La}^{3+}$  to  $\text{Eu}^{3+}$ ), unit cell volumes ranged from  $4377.13(2)$  to  $4639.98(3)$   $\text{\AA}^3$  and crystallized in plate-shaped crystals, and will be referred to as the “parallel phase”. For the “heavy lanthanides” ( $\text{Eu}^{3+}$  to  $\text{Lu}^{3+}$ ) and  $\text{Y}^{3+}$ , unit cell volumes ranged from  $9644.66(3)$  to  $9667.8(3)$   $\text{\AA}^3$  and crystallized in blocky-shaped crystals (Figure 3b), referred to as the “perpendicular phase”. Notice that  $\text{Eu}^{3+}$  is the only lanthanide that crystallizes in both unit cells (Figure 4), with the two phases growing at different rates (vide infra). The most obvious distinction between these two cell types is in the long-range stacking of the  $\text{Cs-Ln}(\text{PW}_{11})_2$  units. The smaller unit cell has  $\text{Cs}$ -

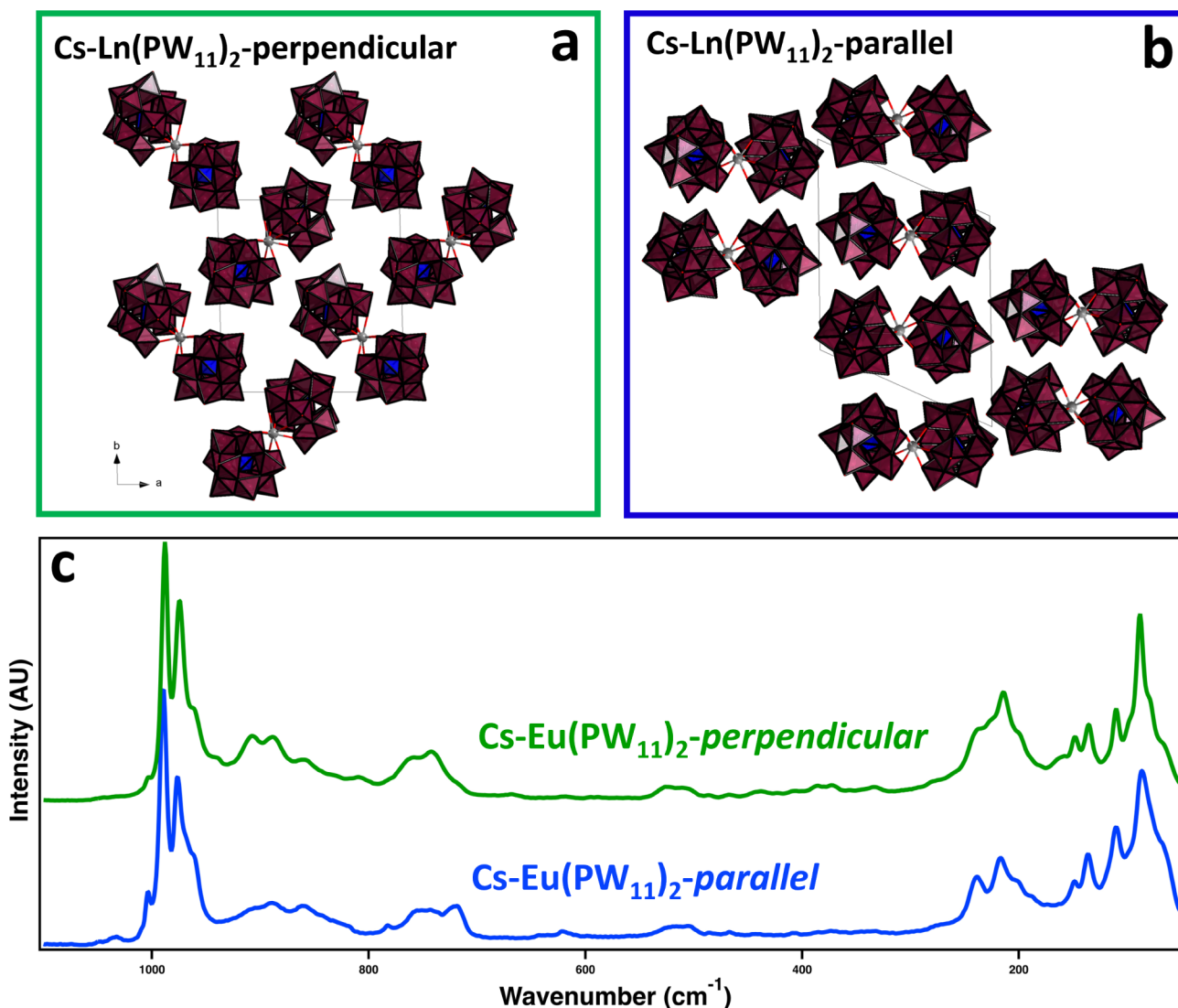


**Figure 4.** Long-range organization of the  $\text{Ln}(\text{PW}_{11})_2$  complexes. a) Perpendicular stacking. b) Parallel stacking. c) Solid-state Raman spectra of the two structure types isolated for the europium complex. The main differences between the two spectra are at lower wavenumbers (between 250 and 50  $\text{cm}^{-1}$ ).

$\text{Ln}(\text{PW}_{11})_2$  complexes parallel to each other, whereas the larger cell has the  $\text{Cs-Ln}(\text{PW}_{11})_2$  units perpendicular to each other (Figure 4a,b). The parallel phase also contains two POM complexes per cell, whereas the perpendicular phase contains four POM complexes per cell. In terms of asymmetric unit, the parallel unit contains only one POM complex versus two for the perpendicular phase. The number of water molecules associated with the  $\text{Ln}(\text{PW}_{11})_2$  complex does not seem to follow any particular trend (Table S2), as often observed for POM compounds.

Raman microscopy analysis was found to be a convenient technique to screen these two phases, as their Raman spectra are generally similar but exhibit distinct features in select regions. For example, the two  $\text{Eu}(\text{PW}_{11})_2$  phases (Figure 4) share the same double bands at  $964\text{--}952 \text{ cm}^{-1}$  ( $\text{W}=\text{O}$  terminal), and the weak bands at around  $897 \text{ cm}^{-1}$  ( $\text{W}-\text{O}-\text{W}$ ). However, only six moderately intense bands below  $250 \text{ cm}^{-1}$  are seen for the parallel phase, whereas seven bands are seen for the perpendicular phase, with the additional band observed at  $226 \text{ cm}^{-1}$  (Figure 4). A closer look at the two different  $\text{Cs-Eu}(\text{PW}_{11})_2$  phases and the larger group overall led to a series of

structural trends. We selected four structural parameters to analyze the  $\text{Cs-M}(\text{PW}_{11})_2$  structures (Figures 2 and 5). First, bending of the complex (abbreviated  $\angle(\text{P}-\text{M}-\text{P})$ , with  $\text{M} = \text{Ln}^{3+}$  or  $\text{An}^{3+}$ ) represented by the angle created between the two POM-encapsulated  $\text{PO}_4^{3-}$  anions and the central cation  $\text{M}^{3+}$ . The second parameter,  $d(\text{P}-\text{P})$ , represents the distance between the two  $\text{PW}_{11}$  ligands, with the positions of the two phosphorus taken as reference. Third, the torsion angle between  $\text{PW}_{11}$  ligands,  $\angle(\text{P}-\text{MO}_8-\text{P})$ , which measures the deviation from a perfect  $D_{4h}$  symmetry for the square antiprismatic coordination of  $\text{Ln}^{3+}$  or  $\text{An}^{3+}$ . Lastly,  $\text{M}-\text{O}$  is the average bond length of the eight metal–oxygen bonds around the central lanthanide ion (or actinide).

Note that these four parameters (Figure 5) could be used for other metal-POM systems.

These four parameters are seemingly related and can be used to describe first- and second-order metal–ligand interactions; as the ionic radius of the central cation decreases, metal–ligand bond lengths should decrease, which should shorten the distance between the two  $\text{PW}_{11}$  ligands. How the  $\text{Cs-Ln}(\text{PW}_{11})_2$  structure compensates for this shortening is then reflected in the

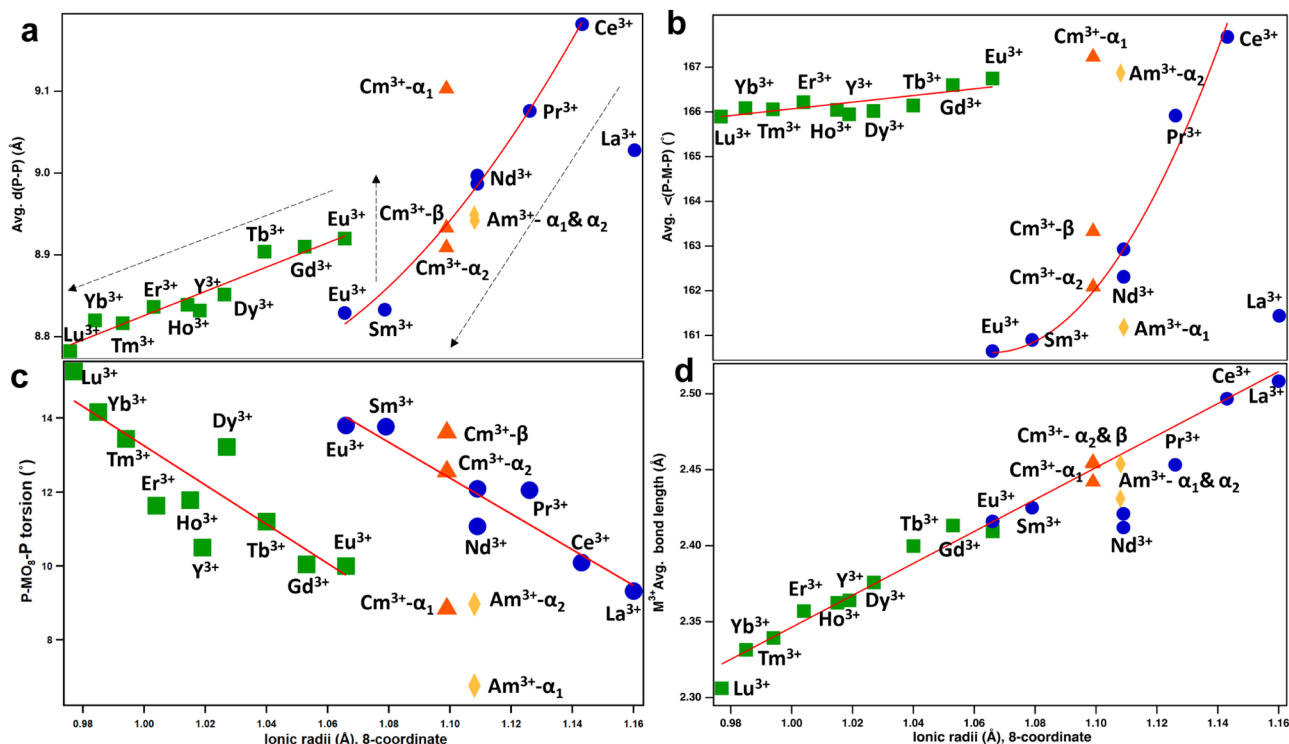


**Figure 5.** Scatter plots are for all structural parameters. a)  $d(P-P)$ , measured distances between the central P atoms within  $\text{Ln}(\text{PW}_{11})_2$ . b)  $\langle(P-\text{M}-\text{P})\rangle$ , measured angles in between the  $\text{PW}_{11}$ . c)  $\langle(P-\text{Mo}_8-\text{P})\rangle$  measures the torsion angle between the  $\text{PW}_{11}$ . d) Lastly, measured bond lengths for the 8-coordinate Ln and An. The dashed arrows in panel a are for eye guidance only. See Table S4 for the numerical values.

bending and/or torsion of the  $\text{PW}_{11}$  complexes and in their long-range stacking. Knowing that all the complexes presented in this study have identical stoichiometry, identical general formula (i.e.,  $\text{Cs}_{11}\text{M}(\text{PW}_{11}\text{O}_{39})_2 \cdot n\text{H}_2\text{O}$ ), identical coordination number, and that the  $\text{PW}_{11}$  POM is rather rigid (relative to organic chelators) and remains tetradentate, the resulting structure morphology is a delicate balance that magnifies subtle effects originating from the metal center (size, electronic structure, covalent nature, etc.).

With the two phases crystallizing, two distinct trends are observed. For the light lanthanides complexes, there is a clear trend from  $\text{Ce}^{3+}$  to  $\text{Eu}^{3+}$ , with a strong shortening of the distance between the  $\text{PW}_{11}$  ligands from 9.182 to 8.829 Å (Figure 5a). As such,  $\text{Cs-Ln}(\text{PW}_{11})_2$  compensates by sharply bending, from  $167.69^\circ$  to  $160.65^\circ$  (Figure 5b), and increasing the torsion angle from  $10.093^\circ$  to  $13.802^\circ$  (Figure 5c). Interestingly,  $\text{Cs-La}(\text{PW}_{11})_2$  does not seem to fit the trend, as there is a shorter-than-expected distance between the two  $\text{PW}_{11}$  ligands of 9.028 Å (Figure 5a) and a higher bent angle of  $161.439^\circ$  (Figure 5b).  $\text{Cs-La}(\text{PW}_{11})_2$  also has a slightly lower cell volume relative to those of the other light lanthanide complexes (Figure 3). It is not obvious why  $\text{La}^{3+}$  might diverge when looking at the other parameters such as the average La–O distance (2.508 Å; Figure 5d) and torsion angle ( $9.320^\circ$ ; Figure 5c), fitting the trends observed for the other light lanthanides.

Unexpectedly, around the size of  $\text{Eu}^{3+}$  (1.066 Å), there is a sudden break within the Ln series (Figure 5) and the  $\text{Cs-Ln}(\text{PW}_{11})_2$  compound undergoes a significant structural reorganization that even translates into a macroscopic change in crystal morphology (Figure 3b). The unit cell volume jumps from  $\sim 4,500$  to  $\sim 9,600$  Å<sup>3</sup> (Figure 3a). This abrupt change between the “pre”- $\text{Eu}(\text{PW}_{11})_2$  complexes and “post”- $\text{Eu}(\text{PW}_{11})_2$  complexes is also visible in the bent angle (Figure 5b), as the

complex reopens by almost  $6^\circ$ , which also increases the distance between the two  $\text{PW}_{11}$  ligands (Figure 5a). The compound also reduces its torsion angle by almost  $5^\circ$  as it accommodates the smaller lanthanide ions (Figure 5c).

Within the subseries of heavy lanthanide complexes ( $\text{Eu}^{3+}$  to  $\text{Lu}^{3+}$ ), the lanthanide contraction is still visible (Figure 5a).  $\text{Y}(\text{PW}_{11})_2$  also behaves like post-Eu lanthanides. The decreasing ionic radius leads to a shorter distance between  $\text{PW}_{11}$ s from 8.920 to 8.783 Å, and, as such,  $\text{Cs-Ln}(\text{PW}_{11})_2$  compensates again by slightly closing the bent angle from  $166.75^\circ$  to  $165.90^\circ$  and increasing the torsion angle from  $10.004^\circ$  to  $15.263^\circ$ . This leads to a situation where some pairs of light and heavy lanthanide complexes, like  $\text{Cs-Pr}(\text{PW}_{11})_2$  and  $\text{Cs-Ho}(\text{PW}_{11})_2$ , exhibit similar local geometries (bent and torsion angles) but yield readily different structure types.

#### Departing from Their Lanthanide Analogues, $\text{Am}(\text{PW}_{11})_2$ and $\text{Cm}(\text{PW}_{11})_2$ Exhibit Distinct Optical and Structural Properties

Thanks to the microscale POM-based synthesis procedure that we recently developed<sup>27</sup> and refined in the present study (Figure 1), only microgram quantities of lanthanide elements are needed for single crystal and bulk characterization of the POM complexes. Extending this approach to relatively high activity<sup>248/246</sup>Cm and<sup>243</sup>Am isotopes allows for a consistent and direct comparison of 4f and 5f elements. Hence, in addition to the lanthanide series mentioned above, we successfully crystallized and characterized three new heavy actinide POM compounds, fully formulated as  $\alpha_1\text{-Cs}_{11}\text{Am}(\text{PW}_{11}\text{O}_{39})_2 \cdot 6\text{H}_2\text{O}$ ,  $\alpha_2\text{-Cs}_{11}\text{Am}(\text{PW}_{11}\text{O}_{39})_2 \cdot 21\text{H}_2\text{O}$ , and  $\alpha_2\text{-Cs}_{11}\text{Cm}(\text{PW}_{11}\text{O}_{39})_2 \cdot 33\text{H}_2\text{O}$ .

The  $\text{Cs-Am}(\text{PW}_{11})_2$  complexes represent the first two trivalent americium POM compounds ever isolated. Interestingly, while the +III oxidation state is the most stable one for

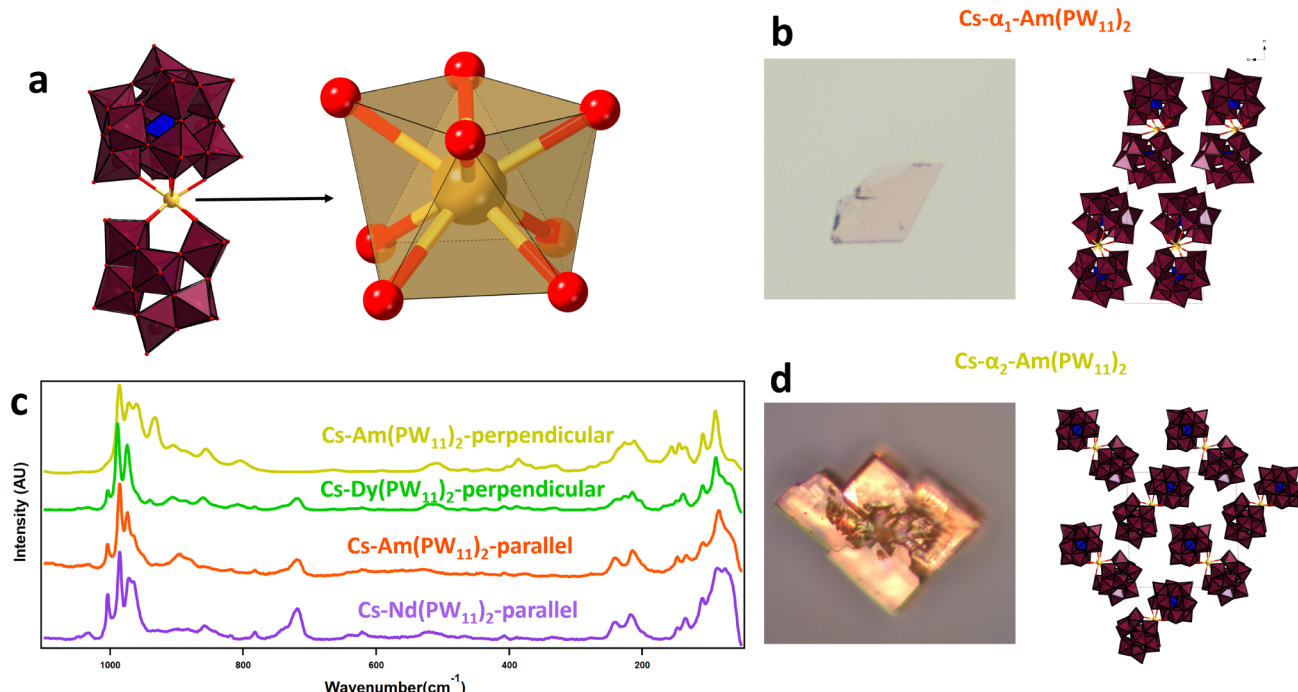


**Figure 6.** Am( $PW_{11}$ )<sub>2</sub> structures. a) View along the  $b$ -axis of the  $\alpha_1$  structure (Cs counterions omitted for clarity) and first coordination sphere of Am<sup>3+</sup>. b) Image of a single crystal of  $\alpha_1$ -Am( $PW_{11}$ )<sub>2</sub>, showing the orange-pink color. c) Comparison of the Raman spectra of the different lattice arrangement, between Nd, Dy, and Am. d) Image of a single crystal of  $\alpha_1$ -Am( $PW_{11}$ )<sub>2</sub>, showing the golden orange color. More crystal images are shown in Figure S6.

americium, no Am(III)-POM compound had been reported. Prior to this study, Sokolova et al.<sup>25</sup> reported in 2009 an Am(IV)-POM, formulated as K<sub>10</sub>H<sub>6</sub>Am( $P_2W_{17}O_{61}$ )<sub>2</sub>·30H<sub>2</sub>O (using potassium persulfate as oxidizer), and Zhang et al.<sup>26</sup> reported in 2023 an Am(V)-POM, formulated as K<sub>x</sub>[ $(CH_3)_2NH_2$ ]<sub>y</sub>(H<sub>3</sub>O)<sub>22-x-y</sub>[ $(AmO_2)Se_6W_{45}O_{159}(H_2O)$ ]<sub>10</sub>·nH<sub>2</sub>O (using Cu<sup>3+</sup> periodate as oxidizer). Both compounds were obtained from milligram-scale syntheses and comparison with the full lanthanide series is impossible since only cerium exhibits the +IV oxidation state and no lanthanide forms species equivalent to the +V americyl ion (under typical aqueous conditions).<sup>35–39</sup> The syntheses of the two Cs-Am( $PW_{11}$ )<sub>2</sub> complexes only used a total of 1.8  $\mu$ g of <sup>243</sup>Am per compound, starting from ~50  $\mu$ L of an Am<sup>3+</sup> stock solution in HNO<sub>3</sub>, and consisted of a one-pot, room-temperature, and fully aqueous synthesis (Figure 1). These examples highlight the advantage of the optimized POM-based strategy as the radiological constraints inherent to highly radioactive isotopes suddenly become manageable when working at the microgram scale.

Cs- $\alpha_1$ -Am( $PW_{11}$ )<sub>2</sub> crystallized in the  $P-1$  space group with a unit cell volume of 4309.69 (19) Å<sup>3</sup>, and Cs- $\alpha_2$ -Am( $PW_{11}$ )<sub>2</sub> crystallized in the same space group with a unit cell volume of 9703.02(2) Å<sup>3</sup> (Figure 3 and Table S1). Interestingly, the Am<sup>3+</sup>-POM crystals appear colorful with relatively high color intensity (see the Supporting Information for additional comments). Raman spectroscopy revealed that the spectrum of Cs- $\alpha_1$ -Am( $PW_{11}$ )<sub>2</sub> is similar to that of the light lanthanides, whereas the spectrum Cs- $\alpha_2$ -Am( $PW_{11}$ )<sub>2</sub> has the similar seven bands below 250 cm<sup>-1</sup> as the heavy lanthanides (Figure 6). Crystals of Cs- $\alpha_1$ -Am( $PW_{11}$ )<sub>2</sub> also exhibit the same plate-like morphology as the light lanthanide analogues, whereas Cs- $\alpha_2$ -Am( $PW_{11}$ )<sub>2</sub> exhibits the same blocky-shaped morphology as the heavy lanthanides. Single crystal XRD analysis confirmed that Cs- $\alpha_1$ -Am( $PW_{11}$ )<sub>2</sub> displays the same parallel stacking as the light lanthanides, while Cs- $\alpha_2$ -Am( $PW_{11}$ )<sub>2</sub> exhibits a perpendicular

stacking formation similar to what is observed for the heavy lanthanides and yttrium (Figure 6b–d).

When comparing the ionic radii to morphological parameters defined in the above section, a strong divergence between Am<sup>3+</sup> (1.108 Å)<sup>40</sup> and its closest size-match Nd<sup>3+</sup> (1.109 Å)<sup>41</sup> is observed (Figures 3–6). The size of Am<sup>3+</sup> would entitle it to form the same phase as Nd<sup>3+</sup> and the other light lanthanides, but it instead forms the additional perpendicular phase like the heavy lanthanides. The behavior of americium is akin to that of europium despite Am<sup>3+</sup> being larger than Eu<sup>3+</sup> (1.066 Å). However, as shown in Figure 5, it is evident that the structural parameters for the two Cs-Am( $PW_{11}$ )<sub>2</sub> structures are specific to americium and do not fit the trends observed along the lanthanide series. It is important to underline that in the structures presented herein, there is no change in the coordination number of the central cation (CN = 8) or its coordination geometry (square antiprismatic). Nonetheless, the distinct nature of the actinide versus lanthanide series is manifested beyond the local coordination of the f-element.

The divergence between the lanthanide and actinide elements is further reinforced with the case of curium (Cm<sup>3+</sup>). We previously published two curium-POM structures: Cs- $\alpha_2$ -Cm( $PW_{11}$ )<sub>2</sub>, fully formulated as  $\alpha_2$ -Cs<sub>11</sub>Cm( $PW_{11}O_{39}$ )<sub>2</sub>·11H<sub>2</sub>O, crystallizes in the monoclinic space group  $P2_1/c$  ( $V$  = 9,013.5(5) Å<sup>3</sup>), and Cs- $\beta$ -Cm( $PW_{11}$ )<sub>2</sub>, formulated as  $\beta$ -Cs<sub>11</sub>Cm( $PW_{11}O_{39}$ )<sub>2</sub>·21.5H<sub>2</sub>O, crystallizes in the monoclinic space group  $P2_1/n$  ( $V$  = 10488.2(6) Å<sup>3</sup>). Following the same procedure, a third phase was isolated for curium. The new phase, named Cs- $\alpha_1$ -Cm( $PW_{11}$ )<sub>2</sub> and fully formulated as  $\alpha_1$ -Cs<sub>11</sub>Cm( $PW_{11}O_{39}$ )<sub>2</sub>·33H<sub>2</sub>O, crystallizes in the triclinic space group  $P-1$  ( $V$  = 5,554.5 Å<sup>3</sup>). Curium is the only f-element for which three different compounds were obtained from the reaction with the PW<sub>11</sub>O<sub>39</sub><sup>7-</sup>. All three structures are unique to curium and could not be anticipated from simple extrapolation from lanthanide chemistry. Not only is curium the only trivalent f-element that

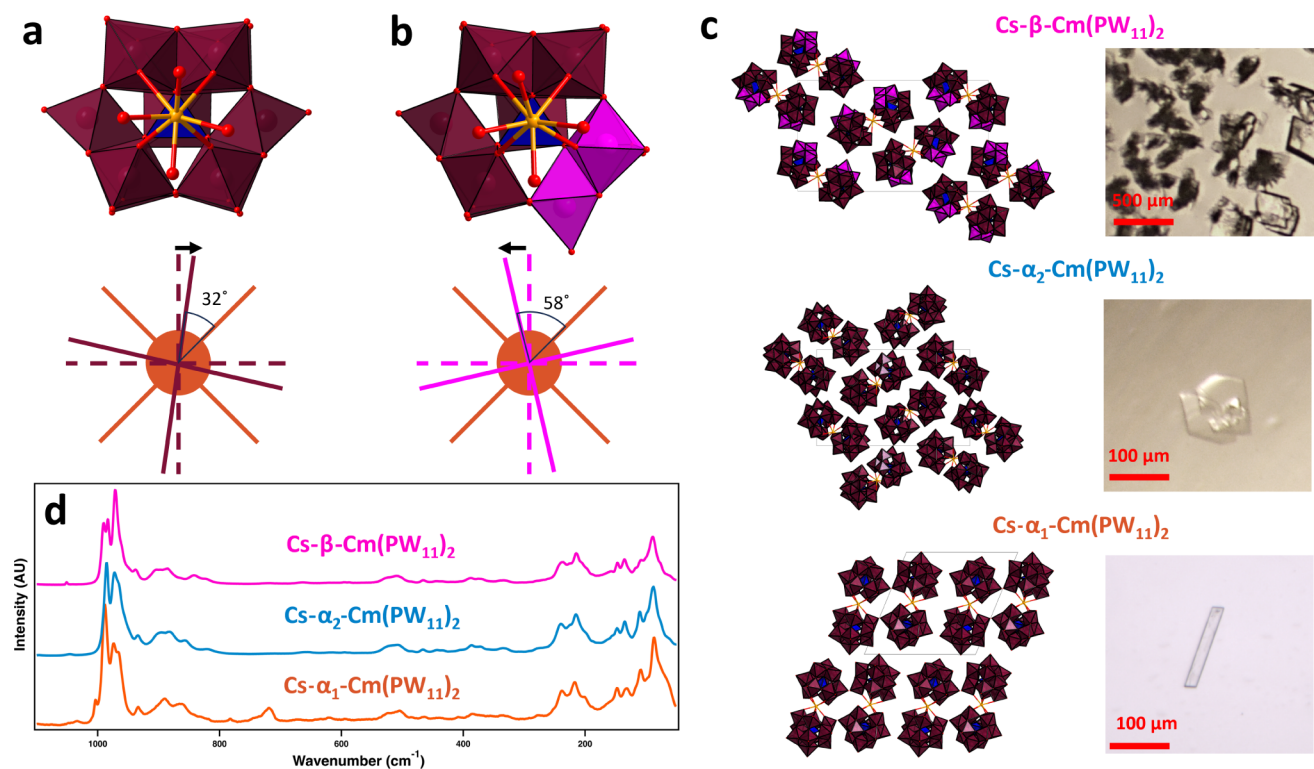


**Figure 7.** Coordination of curium ( $\text{Cm}^{3+}$ ) within the three structure types it forms with the Keggin POM  $\text{PW}_{11}\text{O}_{39}^{7-}$ . a) Top view of the  $\alpha_1$  structure (one of the POM ligands is omitted for clarity). b) Top view of the  $\beta_1$  structure (one of the POM ligands is omitted for clarity). c) Long-range organization of the Cm-POM complexes within the tree structures and associated pictures of the crystals. d) Comparison of the Raman spectra of the Cm-POM tree structures.

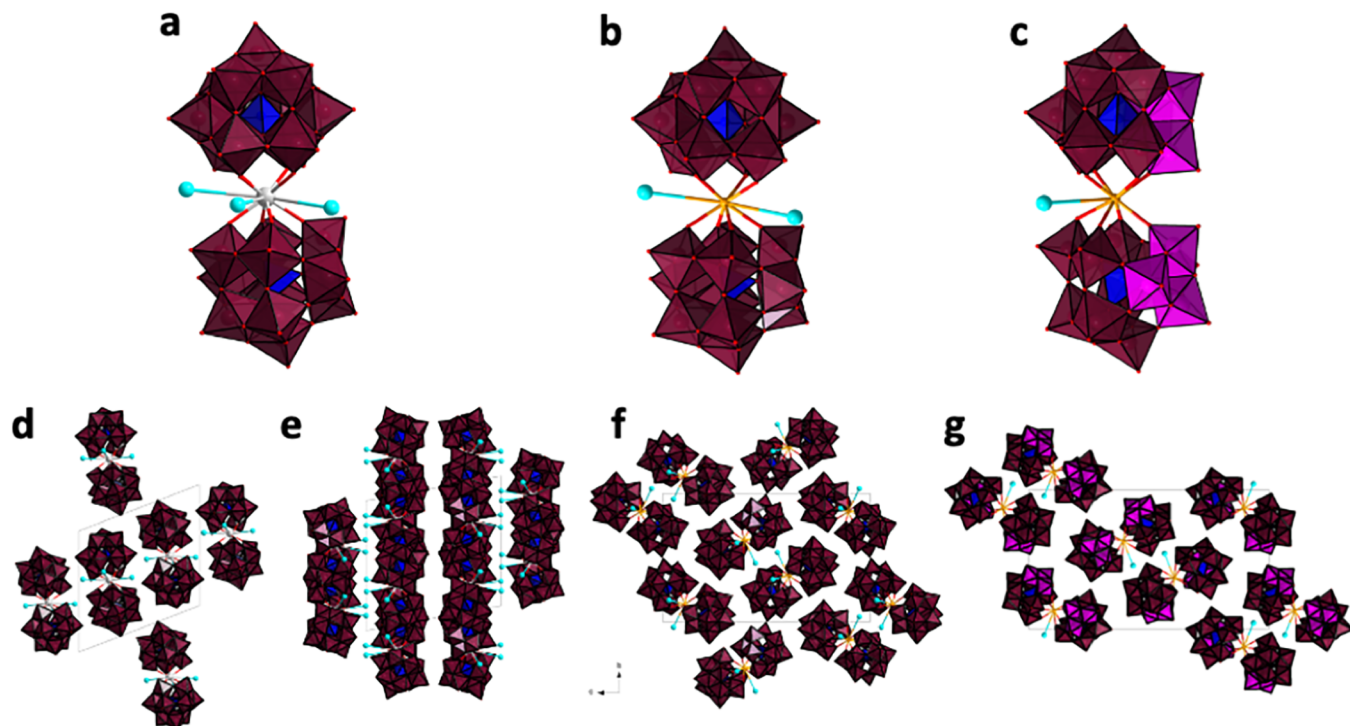


**Figure 8.** Surrounding  $\text{Cs}^+$  ions and their differing frameworks. a) Three  $\text{Cs}^+$  ions surrounding the central  $\text{Ln}$  in  $\text{Ln}(\text{PW}_{11})_2$   $\text{Ln} = \text{La to Lu, Y, Am, Cm}$ ; b) two  $\text{Cs}^+$  surrounding  $\text{Cm}$  in  $\alpha_2\text{-Cm(PW}_{11}\text{)}_2$ ; c) one  $\text{Cs}^+$  surrounding  $\text{Cm}$  in  $\beta\text{-Cm(PW}_{11}\text{)}_2$ ; d) view along  $a$ -axis for the parallel framework; e) view along  $a$ -axis for the perpendicular framework; f) view along  $a$ -axis for the paired perpendicular framework of  $\alpha_2\text{-Cm(PW}_{11}\text{)}_2$ ; g) view along  $a$ -axis for the paired perpendicular framework of  $\beta\text{-Cm(PW}_{11}\text{)}_2$ . For all, W is in maroon polyhedral (rotated trimers are in pink), P in blue polyhedral, O in red spheres,  $\text{Ln}$  in gray,  $\text{Cm}$  in orange, and  $\text{Cs}$  in cyan.

leads the Keggin ion ( $\text{PW}_{11}\text{O}_{39}$ )<sup>7-</sup> to convert into its unusually unstable beta isomer ( $\text{Cs}-\beta\text{-Cm}(\text{PW}_{11})_2$ ) but also the two alpha Keggin complexes that it forms ( $\text{Cs}-\alpha_1\text{-Cm}(\text{PW}_{11})_2$  and  $\text{Cs}-\alpha_2\text{-Cm}(\text{PW}_{11})_2$ ) are unique and depart from what is observed with the lanthanides or americium.

Looking at the two alpha Keggin structures that curium forms ( $\text{Cs}-\alpha_1\text{-Cm}(\text{PW}_{11})_2$  and  $\text{Cs}-\alpha_2\text{-Cm}(\text{PW}_{11})_2$ ), their behavior is somewhat similar to that of  $\text{Eu}^{3+}$ , where the smaller unit cell for both  $\text{Cs-Eu}(\text{PW}_{11})_2$  and  $\text{Cs}-\alpha_1\text{-Cm}(\text{PW}_{11})_2$  features parallel stacking. The larger unit cell features comparable stacking formations; however, in  $\text{Cs}-\alpha_2\text{-Cm}(\text{PW}_{11})_2$ , pairs of  $\text{Cm}(\text{PW}_{11})_2$  stack perpendicular to each other (Figures 7 and S2–S4). While both  $\text{Cs}-\alpha\text{-Cm}(\text{PW}_{11})_2$  phases have similar bond lengths, the perpendicular phase ( $\text{Cs}-\alpha_2\text{-Cm}(\text{PW}_{11})_2$ ) has a smaller  $d(\text{P-P})$  of 8.93 Å, yet a bent angle of 162.71° and a larger torsion angle of 12.55° are observed. The parallel phase ( $\text{Cs}-\alpha_1\text{-Cm}(\text{PW}_{11})_2$ ) has a longer  $d(\text{P-P})$  of 9.103 Å and a larger bent angle of 167.23°, but a smaller torsion angle of 8.85°.

With this morphological context, it becomes easier to understand the crystallization of the  $\text{Cs}-\beta\text{-Cm}(\text{PW}_{11})_2$ , a never-before-seen isomer for  $\text{PW}_{11}$  complexing with a metal ion.<sup>27</sup> The beta isomer of the Keggin ion is normally less thermodynamically stable than the alpha isomer (Figure S1). The  $\text{Cs}-\beta\text{-Cm}(\text{PW}_{11})_2$  shares similar parameters to the perpendicular  $\text{Cs}-\alpha_2\text{-Cm}(\text{PW}_{11})_2$ , with a  $d(\text{P-P})$  of 8.909 Å, a bending of 163.33°, and a torsion of 13.61°. With such similar parameters, a closer look at the crystal structure shows that the rotated trimer in  $[\beta\text{-PW}_{11}\text{O}_{39}]^{7-}$  changes the position of the binding oxygen (Figure 7a,b). Thus, the  $\text{Cs}-\beta\text{-Cm}(\text{PW}_{11})_2$  “twists” to a similar degree as the  $\text{Cs}-\alpha_2\text{-Cm}(\text{PW}_{11})_2$  phase, but in the opposite direction. As such, both  $\text{Cs}-\beta\text{-Cm}(\text{PW}_{11})_2$  and  $\text{Cs}-\alpha_2\text{-Cm}(\text{PW}_{11})_2$  have similar long-range stacking formation and crystal morphology, more plate-shaped (Figure 7c). Raman analysis (Figure 7d) revealed significant differences between the three  $\text{Cs-Cm}(\text{PW}_{11})_2$  structures. Both  $\text{Cs}-\alpha\text{-Cm}(\text{PW}_{11})_2$  structures showcase similar double bands at 964–952 cm<sup>-1</sup> (W=O terminal) and weak bands at around 897 cm<sup>-1</sup> (W–O–W), differentiating only at the lower wavenumber bands. For the perpendicular phase, there are seven bands as opposed to six; however, due to the pairs of  $\text{Cm}(\text{PW}_{11})_2$ , the peak’s intensity is diminished as compared to the heavy  $\text{Cs-Ln}(\text{PW}_{11})_2$  analogues. A similar effect can be seen with the  $\text{Cs}-\beta\text{-Cm}(\text{PW}_{11})_2$  phase; however, for this phase, the most interesting aspect is the double bands at 964–952 cm<sup>-1</sup> (W=O terminal). For  $\text{Cs}-\alpha\text{-Ln/An}(\text{PW}_{11})_2$ , the more intense peak of the double band is at higher wavenumbers, and for  $\text{Cs}-\beta\text{-Cm}(\text{PW}_{11})_2$ , the more intense peak is at lower wavenumbers. Therefore, Raman microscopy can serve as an efficient tool to differentiate between  $\text{PW}_{11}$  isomers and stacking formations in actinide-POM compounds using microcrystals containing submicrogram of the actinide (Figures 6c and 7d).

#### Role of Cesium Ions in Outer-Sphere Coordination and Crystal Packing of $\text{Cs-Ln/An}(\text{PW}_{11}\text{O}_{39})_2$ Complexes

The advantages of our synthesis protocol allowed for probing the effects of  $\text{Cs}^+$  counterions in the lattice formation of a multitude of structures, providing a rare opportunity to assess 4f- and 5f- element chemistry well beyond their first coordination sphere. The structures reported herein (Figures 4, 7, 8, and S3–S4) reveal a higher morphological diversity beyond the central cation’s ( $\text{Ln}^{3+}$  or  $\text{An}^{3+}$ ) first coordination sphere. It is undisputable that the size of Ln or An directs the local geometry for both  $\text{Cs-Ln}(\text{PW}_{11})_2$  and  $\text{Cs-An}(\text{PW}_{11})_2$ , influencing the four

structural parameters defined above (overall length of the complex  $d(\text{P-P})$ , its bending  $\angle(\text{P-M-P})$ , its twisting  $\angle(\text{P-MO}_8\text{-P})$ , and the short-range M–O bond lengths). However, what remains unclear thus far is the influence of the  $\text{Cs}^+$  counterions in the three-component equilibrium f-element/POM/counterion, which is rarely observed in systems with organic ligands. Do the  $\text{Cs}^+$  counterions accommodate the metal–POM interactions by stabilizing the local geometry of  $\text{M}(\text{PW}_{11})_2$ ? Or do changes in the local geometry of  $\text{M}(\text{PW}_{11})_2$  direct  $\text{Cs-M}(\text{PW}_{11})_2$  interactions?

To understand the role that  $\text{Cs}^+$  ions play in the crystallization of  $\text{M}(\text{PW}_{11})_2$ , beyond simple charge-balancing, we analyzed the position of all  $\text{Cs}^+$  ions across all structures (only considering fully occupied  $\text{Cs}^+$ , as such positions would have the most influence or be the most impacted). By measuring  $\text{Cs-M}$  distances ( $\text{M} = \text{Ln}$  or  $\text{An}$ ), a trend emerges, where a subset of  $\text{Cs}^+$  counterions surrounds the f-element and bridges the two  $\text{PW}_{11}$ s (Figure 8). These  $\text{Cs}^+$  cations consistently appear less than 5.5 Å away from the central  $\text{Ln}^{3+}$  or  $\text{An}^{3+}$  cation and feature consistent  $\text{Cs-O}$  bond lengths of 2.977–3.545 Å with a 12 to 14 coordination number. For all  $\text{Ln}(\text{PW}_{11})_2$  structures, as well as  $\alpha_2\text{-Am}(\text{PW}_{11})$  and  $\alpha_1\text{-Cm}(\text{PW}_{11})_2$ , three  $\text{Cs}^+$  positions were consistently encountered around the  $\text{Ln}^{3+}$  or  $\text{An}^{3+}$  cation (Figure 8a). Furthermore, these Cs positions then bridge to neighboring  $\text{M}(\text{PW}_{11})_2$ , completing the framework-like long-range organization observed in those structures. When bridging to the neighboring  $\text{M}(\text{PW}_{11})_2$ ,  $\text{Cs}^+$  binds toward the “end” of the  $\text{M}(\text{PW}_{11})_2$  complex, in other words, furthest away from central f-element. For the  $\text{Ln}(\text{PW}_{11})_2$  ( $\text{Ln} = \text{La}$  to  $\text{Eu}$ ) structures, this results in a parallel framework (Figures 8d and S2). Yet, as the Ln size gets smaller and the corresponding morphological parameters get smaller, maintaining Cs in the same positions seems to become more energetically taxing. Therefore, both a local geometric rearrangement of the  $\text{M}(\text{PW}_{11})_2$  and a lattice rearrangement to the perpendicular framework would be needed, if the same number of Cs positions were maintained (Figures 8e and S3). Thus, the Cs positions around the central  $\text{Ln}^{3+}$  or  $\text{An}^{3+}$  ion serve multiple roles: they stabilize the geometry of  $\text{M}(\text{PW}_{11})_2$ , and they minimize complex–complex interactions, while simultaneously increasing  $\text{Cs-PW}_{11}$  interactions. When comparing all of the lanthanide and actinide compounds reported herein, changing the nature of a single ion (i.e., the central  $\text{Ln}^{3+}$  or  $\text{An}^{3+}$  cation) seems to reverberate across these large structures, hence providing a magnifying lens to pinpoint subtle differences with the f-element series.

The uniquely high number of structures Cm can accommodate highlights the various roles Cs can play in the delicate balance among the f-elements, POM, and counterions. The  $\alpha_1\text{-Cm}(\text{PW}_{11})_2$  features three surrounding Cs ions (similar to  $\text{Ln}(\text{PW}_{11})_2$   $\text{Ln} = \text{La}$  to  $\text{Eu}$ ),  $\alpha_2\text{-Cm}(\text{PW}_{11})_2$  has two Cs positions, and  $\beta\text{-Cm}(\text{PW}_{11})_2$  only has one (Figure 8c, d). The last two Cm structures feature perpendicular stacking of pairs of  $\text{Cm}(\text{PW}_{11})_2$  complexes (Figure 8f, g). The lower number of surrounding Cs seemingly corresponds to higher complex–complex interactions. Furthermore, a closer look at the  $\beta\text{-Cm}(\text{PW}_{11})_2$  and  $\alpha_2\text{-Cm}(\text{PW}_{11})_2$  structures reveals  $\beta\text{-Cm}(\text{PW}_{11})_2$ ’s lone Cs position. Cm is the only metal thus far that has been able to accommodate the beta isomer, which is hypothesized to occur through the stabilization of the rotated trimer at structural parameters similar to those of its  $\alpha_2\text{-Cm}(\text{PW}_{11})_2$  counterpart. Yet,  $\beta\text{-Cm}(\text{PW}_{11})_2$  still has only one Cs position, which is suspected to come at the cost of the trimer rotation. It is thus more likely that the  $\text{Cs}^+$  promotes the isomerization of the  $\text{PW}_{11}$ , while the  $\text{Cm}^{3+}$  ion

allows for the stabilization and crystallization of the new geometry (Figures 8g and S4).

## CONCLUSION

This study clearly shows that trivalent lanthanides and heavy actinides display distinct coordination chemistries. The series of POM/f-element complexes isolated constitutes a rare and comprehensive example where all the studied cations, from  $\text{La}^{3+}$  to  $\text{Lu}^{3+}$ , plus  $\text{Y}^{3+}$ ,  $\text{Am}^{3+}$ , and  $\text{Cm}^{3+}$ , are confined with the same metal–ligand unit and exhibit the same 8-coordinated local geometry, while yielding significant structural differences at a longer range (i.e., bending and twisting of the POM/f-element complex, complex–complex arrangement, and complex vs counterion positions). The lanthanide elements form two distinct crystal structure types: one with the  $\text{M}(\text{POM})_2$  complexes organized in a parallel manner and one where complexes are perpendicular. The lanthanide series undergoes a clear structural break at europium (the only lanthanide forming the two structures). Surprisingly, the heavy actinides  $\text{Am}^{3+}$  and  $\text{Cm}^{3+}$  depart from their lanthanide analogues and yield structures with their own specificities. Americium forms two structures, akin to europium, but does not fit the structural trends observed for lanthanides. Curium emphasizes further the distinct chemistries of trivalent lanthanides and actinides, being the only f-element that yields three different structure types ( $\alpha$ ,  $\alpha_2$ , and  $\beta$ ). These three structures are unique to curium and could not be anticipated from extrapolation from lanthanide or americium chemistry. The particularities of the POM chelating platform studied here allow for studying both 4f and 5f cations under identical conditions and magnifying differences among these elements that are typically difficult to observe with traditional ligands. The compounds reported here represent a first step toward expanding actinide-POM chemistry, and work is ongoing to apply the methods detailed here to other POMs and other difficult-to-study elements.

## EXPERIMENTAL SECTION

### Caution!

<sup>248/247/246</sup>Cm and <sup>243</sup>Am, as well as their decay products, constitute serious health hazards, because of their radioactive and chemical properties. All experiments involving radionuclides were conducted at Lawrence Livermore National Laboratory, in facilities designed for the safe handling of long-lived and short-lived radioactive materials and associated waste.

### Materials

Curium samples (97% <sup>248</sup>Cm + 3% <sup>246</sup>Cm + 0.01% <sup>247</sup>Cm) were prepared from a primary source purchased from Oak Ridge National Laboratory (USA) and <sup>243</sup>Am(III) chloride purchased from Eckert and Ziegler (USA). NaCH<sub>3</sub>COO (>99.9%), cesium chloride (>99.99%), Na<sub>2</sub>WO<sub>4</sub>×2H<sub>2</sub>O (>99%), phosphoric acid, and lanthanide trichloride salts (>99.9%) were purchased from chemical providers (VWR and Millipore Sigma) and used as received. All solutions were prepared using deionized water purified by reverse osmosis cartridge system (>18.2 MΩ·cm). All experiments were performed in a temperature-controlled room (22 °C).

### Synthesis

Lanthanide or actinide chloride salts (<sup>246/248</sup>Cm<sup>3+</sup>/<sup>243</sup>Am<sup>3+</sup> from a parent stock solution in HCl) are added to a 200 μM PW<sub>11</sub> solution in 0.1 M acetate buffer at pH 5.5. A 1:2 stoichiometric addition of lanthanide or actinide to PW<sub>11</sub> (concentrations for lanthanides and actinides were kept in the 50–100 μM range). For crystallization, 6 M CsCl is titrated in 5–50 μL to 1:2 stoichiometric solutions (10 to 100 μL, at pH 5.5, 100 mM acetate buffer). After 1–5 days of ambient conditions, several single crystals of Ln-PW<sub>11</sub> are visible to the naked

eye. Upon inspection with an optical microscope, XRD quality crystals are mounted and characterized via small molecule single crystal XRD, while the rest are kept for Raman microscopy.

### Crystallographic Studies

The Cs-Ln(PW<sub>11</sub>)<sub>2</sub>, Cs-Cm(PW<sub>11</sub>)<sub>2</sub>, and Cs-Am(PW<sub>11</sub>)<sub>2</sub> structures were collected in one of LLNL's radiochemistry laboratories using a Rigaku Synergy Custom single crystal diffractometer, equipped with a kappa goniometer, and using Mo Kα radiation ( $\lambda = 0.71073 \text{ \AA}$ ) with a FWHM of ~200 μm at the sample from a MicroMax-007 HF microfocus rotating anode source. Images were recorded on a Dectris Pilatus 3R (300K – CdTe) detector and processed using CrysAlis<sup>Pro</sup>. After integration, both analytical absorption and empirical absorption (spherical harmonic, image scaling, and detector scaling) corrections were applied.<sup>42</sup> All structures were solved by the intrinsic phasing method from SHELXT program,<sup>43</sup> developed by successive difference Fourier syntheses, and refined by full-matrix least-squares on all F<sup>2</sup> data using SHELX<sup>44</sup> via OLEX2 interface.<sup>45</sup> Crystallographic information for the six reported structures can be obtained free of charge from the Cambridge Crystallographic Data Center (<https://www.ccdc.cam.ac.uk/>) upon referencing CCDC numbers in crystallographic Table S1.

### Raman Microscopy

Raman spectra were collected using a Senterra II confocal Raman microscope (Bruker), equipped with high-resolution gratings (1,200 lines/mm) and a 532 nm laser source (operated at 15 mW), and a TE-cooled CCD detector. Reported spectra are the average of at least 2–5 different spots per sample, each spot analysis consisting of 2 binned 16 scans. The integration time was set to 400 ms per scan. No damage to the sample was observed due to laser irradiation. Background spectra of the glass slides with paratone oil showed two peaks at 1010 cm<sup>-1</sup> and at 750 cm<sup>-1</sup>.

## ASSOCIATED CONTENT

### Supporting Information

The Supporting Information is available free of charge at <https://pubs.acs.org/doi/10.1021/jacsau.4c00245>.

Summary of structures obtained, list of chemical formula and associated CCDC numbers, materials and methods, comments on the AmPOM crystal optical properties, comments on bond valence sum calculations, detailed XRD data collection information (Tables S1–S4), XRD data analysis information (Table S5), bond valence sum values (Tables S6–S7), additional structural visualizations (Figures S1–S4), additional microscopy pictures of the crystal (Figure S5), Raman spectra (Figure S6), and references (PDF)

Finalized CIF files (ZIP)

Crystallographic data (ZIP)

## AUTHOR INFORMATION

### Corresponding Authors

Ian Colliard – Physical and Life Sciences Directorate, Glenn T. Seaborg Institute, Lawrence Livermore National Laboratory, Livermore, California 94550, United States; Material Sciences Division, Lawrence Livermore National Laboratory, Livermore, California 94550, United States; [orcid.org/0000-0003-1883-1155](https://orcid.org/0000-0003-1883-1155); Email: [Colliard1@LLNL.gov](mailto:Colliard1@LLNL.gov)

Gauthier J.-P. Deblonde – Physical and Life Sciences Directorate, Glenn T. Seaborg Institute, Lawrence Livermore National Laboratory, Livermore, California 94550, United States; Nuclear and Chemical Sciences Division, Lawrence Livermore National Laboratory, Livermore, California 94550, United States; [orcid.org/0000-0002-0825-8714](https://orcid.org/0000-0002-0825-8714); Email: [Deblonde1@LLNL.gov](mailto:Deblonde1@LLNL.gov)

Complete contact information is available at:  
<https://pubs.acs.org/10.1021/jacsau.4c00245>

## Author Contributions

CRediT: Ian Colliard conceptualization, data curation, formal analysis, investigation, writing-original draft, writing-review & editing; Gauthier J.-P. Deblonde conceptualization, data curation, formal analysis, funding acquisition, investigation, project administration, resources, supervision, writing-original draft, writing-review & editing.

## Notes

The authors declare no competing financial interest.

## ACKNOWLEDGMENTS

This material is based upon work supported by the U.S. Department of Energy, Office of Science, Office of Basic Energy Sciences, Heavy Element Chemistry program at Lawrence Livermore National Laboratory under Contract DE-AC52-07NA27344. G.J.-P.D. acknowledges support from the LDRD program at LLNL for initial tests and procurement of the POM starting materials. Release number: LLNL-JRNL-861782. I.C. thanks Josh W. and Ozzy O. for their insightful discussions. G.J.-P.D. thanks Marie F. and Holly D. for inspiring discussions.

## REFERENCES

- (1) Seaborg, G. T. The Transuranium Elements. *Science* **1946**, *104* (2704), 379–386.
- (2) Groom, C. R.; Bruno, I. J.; Lightfoot, M. P.; Ward, S. C. The Cambridge Structural Database. *Acta Cryst. B* **2016**, *72* (2), 171–179.
- (3) Arnold, P. L.; Dutkiewicz, M. S.; Walter, O. Organometallic Neptunium Chemistry. *Chem. Rev.* **2017**, *117* (17), 11460–11475.
- (4) Roberto, J. B.; Alexander, C. W.; Boll, R. A.; Burns, J. D.; Ezold, J. G.; Felker, L. K.; Hogle, S. L.; Rykaczewski, K. P. Actinide Targets for the Synthesis of Super-Heavy Elements. *Nucl. Phys. A* **2015**, *944*, 99–116.
- (5) Durbin, P. W. Metabolism and Biological Effects of the Transplutonium Elements. In Uranium · Plutonium Transplutonic Elements. In *Handbuch der experimentellen Pharmakologie/Handbook of Experimental Pharmacology*, Hodge, H. C.; Hursh, J. B.; Stannard, J. N.; Springer: Berlin, Heidelberg, 1973; pp. 739896.
- (6) Ménétrier, F.; Taylor, D. M.; Comte, A. The Biokinetics and Radiotoxicology of Curium: A Comparison with Americium. *Appl. Radiat. Isot.* **2008**, *66* (5), 632–647.
- (7) Sykora, R. E.; Assefa, Z.; Haire, R. G.; Albrecht-Schmitt, T. E. First Structural Determination of a Trivalent Californium Compound with Oxygen Coordination. *Inorg. Chem.* **2006**, *45* (2), 475–477.
- (8) Cary, S. K.; Vasiliu, M.; Baumbach, R. E.; Stritzinger, J. T.; Green, T. D.; Diefenbach, K.; Cross, J. N.; Knappenberger, K. L.; Liu, G.; Silver, M. A.; DePrince, A. E.; Polinski, M. J.; Cleve, S. M. V.; House, J. H.; Kikugawa, N.; Gallagher, A.; Arico, A. A.; Dixon, D. A.; Albrecht-Schmitt, T. E. Emergence of Californium as the Second Transitional Element in the Actinide Series. *Nat. Commun.* **2015**, *6* (1), 6827.
- (9) Silver, M. A.; Cary, S. K.; Johnson, J. A.; Baumbach, R. E.; Arico, A. A.; Luckey, M.; Urban, M.; Wang, J. C.; Polinski, M. J.; Chemey, A.; Liu, G.; Chen, K.-W.; Cleve, S. M. V.; Marsh, M. L.; Eaton, T. M.; Burgt, L. J. V. D.; Gray, A. L.; Hobart, D. E.; Hanson, K.; Maron, L.; Gendron, F.; Autschbach, J.; Speldrich, M.; Kögerler, P.; Yang, P.; Braley, J.; Albrecht-Schmitt, T. E. Characterization of Berkelium(III) Dipicolinate and Borate Compounds in Solution and the Solid State. *Science* **2016**, *353* (6302), aaf3762.
- (10) Silver, M. A.; Cary, S. K.; Garza, A. J.; Baumbach, R. E.; Arico, A. A.; Galmin, G. A.; Chen, K.-W.; Johnson, J. A.; Wang, J. C.; Clark, R. J.; et al. Electronic Structure and Properties of Berkelium Iodates. *J. Am. Chem. Soc.* **2017**, *139* (38), 13361–13375.
- (11) Galley, S. S.; Pattenade, S. A.; Gaggioli, C. A.; Qiao, Y.; Sperling, J. M.; Zeller, M.; Pakhira, S.; Mendoza-Cortes, J. L.; Schelter, E. J.; Albrecht-Schmitt, T. E.; et al. Synthesis and Characterization of Tris-Chelate Complexes for Understanding f-Orbital Bonding in Later Actinides. *J. Am. Chem. Soc.* **2019**, *141* (6), 2356–2366.
- (12) Cary, S. K.; Su, J.; Galley, S. S.; Albrecht-Schmitt, T. E.; Batista, E. R.; Ferrier, M. G.; Kozimor, S. A.; Mocko, V.; Scott, B. L.; Van Alstine, C. E.; et al. A Series of Dithiocarbamates for Americium, Curium, and Californium. *Dalton Trans.* **2018**, *47* (41), 14452–14461.
- (13) Sperling, J. M.; Warzecha, E.; Windorff, C. J.; Klamm, B. E.; Gaiser, A. N.; Whitefoot, M. A.; White, F. D.; Poe, T. N.; Albrecht-Schönzart, T. E. Pressure-Induced Spectroscopic Changes in a Californium 1D Material Are Twice as Large as Found in the Holmium Analog. *Inorg. Chem.* **2020**, *59* (15), 10794–10801.
- (14) Sperling, J. M.; Beck, N.; Scheibe, B.; Bai, Z.; Brannon, J.; Gomez-Martinez, D.; Grödler, D.; Johnson, J. A.; Lin, X.; Rotermund, B. M.; Albrecht-Schönzart, T. E. S. Synthesis, characterization, and high-pressure studies of a 3D berkelium(iii) carboxylate framework material. *Chem. Commun.* **2022**, *58* (13), 2200–2203.
- (15) Gaiser, A. N.; Celis-Barros, C.; White, F. D.; Beltran-Leiva, M. J.; Sperling, J. M.; Salpage, S. R.; Poe, T. N.; Jian, T.; Wolford, N. J.; Jones, N. J.; et al. Creation of an Unexpected Plane of Enhanced Covalency in Cerium(III) and Berkelium(III) Terpyridyl Complexes. *Nat. Commun.* **2021**, *12* (1), 7230.
- (16) Goodwin, C. A. P.; Su, J.; Stevens, L. M.; White, F. D.; Anderson, N. H.; Auxier, J. D.; Albrecht-Schönzart, T. E.; Batista, E. R.; Briscoe, S. F.; Cross, J. N.; et al. Isolation and Characterization of a Californium Metallocene. *Nature* **2021**, *599* (7885), 421–424.
- (17) Brenner, N.; Sperling, J. M.; Poe, T. N.; Celis-Barros, C.; Brittain, K.; Villa, E. M.; Albrecht-Schmitt, T. E.; Polinski, M. J. Trivalent F-Element Squarates, Square-Oxalates, and Cationic Materials, and the Determination of the Nine-Coordinate Ionic Radius of Cf(III). *Inorg. Chem.* **2020**, *59* (13), 9384–9395.
- (18) Sperling, J. M.; Warzecha, E. J.; Celis-Barros, C.; Sergentu, D.-C.; Wang, X.; Klamm, B. E.; Windorff, C. J.; Gaiser, A. N.; White, F. D.; Beery, D. A.; et al. Compression of Curium Pyrrolidine-Dithiocarbamate Enhances Covalency. *Nature* **2020**, *583* (7816), 396–399.
- (19) Long, B. N.; Sperling, J. M.; Windorff, C. J.; Albrecht-Schönzart, T. E. Characterization of the Organoamericium Complex Cp'3Am. *Organometallics* **2023**, *42* (21), 3048–3052.
- (20) Long, B. N.; Beltrán-Leiva, M. J.; Sperling, J. M.; Poe, T. N.; Celis-Barros, C.; Albrecht-Schönzart, T. E. Altering the Spectroscopy, Electronic Structure, and Bonding of Organometallic Curium(III) upon Coordination of 4,4'-bipyridine. *Nat. Commun.* **2023**, *14* (1), 3774.
- (21) Cary, S. K.; Silver, M. A.; Liu, G.; Wang, J. C.; Bogart, J. A.; Stritzinger, J. T.; Arico, A. A.; Hanson, K.; Schelter, E. J.; Albrecht-Schmitt, T. E. Spontaneous Partitioning of Californium from Curium: Curious Cases from the Crystallization of Curium Coordination Complexes. *Inorg. Chem.* **2015**, *54* (23), 11399–11404.
- (22) Arteaga, A.; Nicholas, A. D.; Ducati, L. C.; Autschbach, J.; Surbella, R. G. I. Americium Oxalate: An Experimental and Computational Investigation of Metal–Ligand Bonding. *Inorg. Chem.* **2023**, *62* (12), 4814–4822.
- (23) Arteaga, A.; Nicholas, A. D.; Sinnwell, M. A.; McNamara, B. K.; Buck, E. C.; Surbella, R. G. I. Expanding the Transuranic Metal–Organic Framework Portfolio: The Optical Properties of Americium(III) MOF-76. *Inorg. Chem.* **2023**, *62*, 21036.
- (24) Poe, T. N.; Ramanantoanina, H.; Sperling, J. M.; Wineinger, H. B.; Rotermund, B. M.; Brannon, J.; Bai, Z.; Scheibe, B.; Beck, N.; Long, B. N.; et al. Isolation of a Californium(II) Crown–Ether Complex. *Nat. Chem.* **2023**, *15* (5), 722–728.
- (25) Sokolova, M. N.; Fedossev, A. M.; Andreev, G. B.; Budantseva, N. A.; Yusov, A. B.; Moisy, P. Synthesis and Structural Examination of Complexes of Am(IV) and Other Tetravalent Actinides with Lacunary Heteropolyanion A<sub>2</sub>P<sub>2</sub>W<sub>17</sub>O<sub>61</sub>–. *Inorg. Chem.* **2009**, *48* (19), 9185–9190.
- (26) Zhang, H.; Li, A.; Li, K.; Wang, Z.; Xu, X.; Wang, Y.; Sheridan, M. V.; Hu, H.-S.; Xu, C.; Alekseev, E. V.; et al. Ultrafiltration

Separation of Am(VI)-Polyoxometalate from Lanthanides. *Nature* **2023**, *616* (7957), 482–487.

(27) Colliard, I.; Lee, J. R. I.; Colla, C. A.; Mason, H. E.; Sawvel, A. M.; Zavarin, M.; Nyman, M.; Deblonde, G. J.-P. Polyoxometalates as Ligands to Synthesize, Isolate and Characterize Compounds of Rare Isotopes on the Microgram Scale. *Nat. Chem.* **2022**, *14* (12), 1357–1366.

(28) Kimura, T.; Choppin, G. R.; Kato, Y.; Yoshida, Z. Determination of the Hydration Number of Cm(III) in Various Aqueous Solutions. *Radiochim. Acta* **1996**, *72* (2), 61–64.

(29) Kimura, T.; Nagaishi, R.; Kato, Y.; Yoshida, Z. Luminescence Study on Solvation of Americium(III), Curium(III) and Several Lanthanide(III) Ions in Nonaqueous and Binary Mixed Solvents. *Radiochim. Acta* **2001**, *89* (3), 125–130.

(30) Colla, C. A.; Colliard, I.; Sawvel, A. M.; Nyman, M.; Mason, H. E.; Deblonde, G. J.-P. Contrasting Trivalent Lanthanide and Actinide Complexation by Polyoxometalates via Solution-State NMR. *Inorg. Chem.* **2023**, *62* (16), 6242–6254.

(31) Gumerova, N. I.; Rompel, A. Speciation Atlas of Polyoxometalates in Aqueous Solutions. *Sci. Adv.* **2023**, *9* (25), No. eadi0814.

(32) Gumerova, N. I.; Rompel, A. Polyoxometalates in Solution: Speciation under Spotlight. *Chem. Soc. Rev.* **2020**, *49* (21), 7568–7601.

(33) Zhang, C.; Howell, R. C.; Scotland, K. B.; Perez, F. G.; Todaro, L.; Francesconi, L. C. Aqueous Speciation Studies of Europium(III) Phosphotungstate. *Inorg. Chem.* **2004**, *43* (24), 7691–7701.

(34) Lundberg, D.; Persson, I. The Size of Actinoid(III) Ions – Structural Analysis vs. Common Misinterpretations. *Coord. Chem. Rev.* **2016**, *318*, 131–134.

(35) Rice, N. T.; Popov, I. A.; Russo, D. R.; Bacsa, J.; Batista, E. R.; Yang, P.; Telser, J.; La Pierre, H. S. Design, Isolation, and Spectroscopic Analysis of a Tetravalent Terbium Complex. *J. Am. Chem. Soc.* **2019**, *141* (33), 13222–13233.

(36) Ramanathan, A.; Kaplan, J.; Sergentu, D.-C.; Branson, J. A.; Ozerov, M.; Kolesnikov, A. I.; Minasian, S. G.; Autschbach, J.; Freeland, J. W.; Jiang, Z.; et al. et al. Chemical Design of Electronic and Magnetic Energy Scales of Tetravalent Praseodymium Materials. *Nat. Commun.* **2023**, *14* (1), 3134.

(37) Gompa, T. P.; Ramanathan, A.; Rice, N. T.; Pierre, H. S. L. The Chemical and Physical Properties of Tetravalent Lanthanides: Pr, Nd, Tb, and Dy. *Dalton Trans.* **2020**, *49* (45), 15945–15987.

(38) Palumbo, C. T.; Zivkovic, I.; Scopelliti, R.; Mazzanti, M. Molecular Complex of Tb in the + 4 Oxidation State. *J. Am. Chem. Soc.* **2019**, *141* (25), 9827–9831.

(39) Shafi, Z.; Gibson, J. K. Lanthanide Complexes Containing a Terminal Ln=O Oxo Bond: Revealing Higher Stability of Tetravalent Praseodymium versus Terbium. *Inorg. Chem.* **2022**, *61* (18), 7075–7087.

(40) Cross, J. N.; Villa, E. M.; Wang, S.; Diwu, J.; Polinski, M. J.; Albrecht-Schmitt, T. E. S. Syntheses, Structures, and Spectroscopic Properties of Plutonium and Americium Phosphites and the Redetermination of the Ionic Radii of Pu(III) and Am(III). *Inorg. Chem.* **2012**, *51* (15), 8419–8424.

(41) Shannon, R. D. Revised Effective Ionic Radii and Systematic Studies of Interatomic Distances in Halides and Chalcogenides. *Acta Crystallogr.* **1976**, A32, 751–767.

(42) Sheldrick, G. M. SADABS, *Bruker-Siemens Area Detection Absorption Other Correction*. Version 2008/1. Bruker: Madison, 2008.

(43) Sheldrick, G. M. SHELTXT – Integrated Space-Group and Crystal-Structure Determination. *Acta Cryst. A* **2015**, *71* (1), 3–8.

(44) Sheldrick, G. M. A Short History of SHELT. *Acta Cryst. A* **2008**, *64* (1), 112–122.

(45) Dolomanov, O. V.; Bourhis, L. J.; Gildea, R. J.; Howard, J. A. K.; Puschmann, H. OLEX2: A Complete Structure Solution, Refinement and Analysis Program. *J. Appl. Crystallogr.* **2009**, *42* (2), 339–341.